British Journal of Cancer www.nature.com/bjc

ARTICLE OPEN

Check for updates

Cellular and Molecular Biology

Peroxisomal β-oxidation enzyme, DECR2, regulates lipid metabolism and promotes treatment resistance in advanced prostate cancer

Chui Yan Mah[1,2], An Dieu Trang Nguyen[1,2], Takuto Niijima[1], Madison Helm[1,2], Jonas Dehairs[3], Feargal J. Ryan[2,4], Natalie Ryan[1,2], Lake-Ee Quek[5], Andrew J. Hoy[5], Anthony S. Don[5], Ian G. Mills[6,7], Johannes V. Swinnen[3], David J. Lynn[2,4], Zeyad D. Nassar[1,2]✉ and Lisa M. Butler[1,2]✉

BACKGROUND: Peroxisomes are central metabolic organelles that have key roles in fatty acid homoeostasis. As prostate cancer (PCa) is particularly reliant on fatty acid metabolism, we explored the contribution of peroxisomal β-oxidation (perFAO) to PCa viability and therapy response.

METHODS: Bioinformatic analysis was performed on clinical transcriptomic datasets to identify the perFAO enzyme, 2,4-dienoyl CoA reductase 2 (DECR2) as a target gene of interest. Impact of DECR2 and perFAO inhibition via thioridazine was examined in vitro, in vivo, and in clinical prostate tumours cultured ex vivo. Transcriptomic and lipidomic profiling was used to determine the functional consequences of DECR2 inhibition in PCa.

RESULTS: DECR2 is upregulated in clinical PCa, most notably in metastatic castrate-resistant PCa (CRPC). Depletion of DECR2 significantly suppressed proliferation, migration, and 3D growth of a range of CRPC and therapy-resistant PCa cell lines, and inhibited LNCaP tumour growth and proliferation in vivo. DECR2 influences cell cycle progression and lipid metabolism to support tumour cell proliferation. Further, co-targeting of perFAO and standard-of-care androgen receptor inhibition enhanced suppression of PCa cell proliferation.

CONCLUSION: Our findings support a focus on perFAO, specifically DECR2, as a promising therapeutic target for CRPC and as a novel strategy to overcome lethal treatment resistance.

British Journal of Cancer (2024) 130:741–754; https://doi.org/10.1038/s41416-023-02557-8

INTRODUCTION

Prostate cancer (PCa) remains the most diagnosed malignancy and the leading cause of cancer-related deaths in men globally [1]. One of the main hurdles for the treatment of PCa is overcoming resistance to current androgen-targeting agents, which form the mainstay of therapy for locally advanced and metastatic PCa. Despite the development of potent androgen receptor (AR) pathway inhibitors, including enzalutamide (ENZ), these agents are not curative and patients with castrate-resistant prostate cancer (CRPC) eventually succumb to this disease. Targeting cancer metabolism has gained increasing attention as an attractive strategy to overcome resistance to AR-targeted therapies [2].

Altered lipid metabolism is a well-characterised hallmark of PCa and, accordingly, significant research efforts have been made to target de novo lipogenesis and lipid uptake pathways [3, 4]. Now there is a growing body of evidence that implicates fatty acid oxidation (FAO, or β-oxidation) as a critical aspect of lipid metabolism that drives PCa progression and treatment resistance [5–8], irrespective of fatty acid source. Despite the complexity of the FAO pathway, most drug development approaches have focused entirely on targeting mitochondrial carnitine palmitoyltransferase I (CPT1), the rate-limiting enzyme of mitochondrial β-oxidation. Indeed, our previous work demonstrated therapeutic efficacy in targeting mitochondrial β-oxidation using a pharmacological agent, etomoxir (CPT1 inhibitor) in patient-derived explants (PDEs) [8]. With this observation, we also uncovered a novel target of mitochondrial β-oxidation, DECR1, the rate-limiting enzyme of an auxiliary pathway of polyunsaturated fatty acid (PUFA) oxidation [8]. On the basis of this discovery, we were motivated to investigate and characterise its peroxisomal counterpart, peroxisomal 2,4-dienoyl-CoA reductase 2 (DECR2), and its role in PCa.

[1]South Australian Immunogenomics Cancer Institute and Freemasons Centre for Male Health and Wellbeing, University of Adelaide, Adelaide, SA, Australia. [2]Precision Cancer Medicine Theme, South Australian Health and Medical Research Institute, Adelaide, SA, Australia. [3]Department of Oncology, Laboratory of Lipid Metabolism and Cancer, KU Leuven, Leuven, Belgium. [4]Flinders Health and Medical Research Institute, Flinders University, Bedford Park, SA, Australia. [5]School of Medical Sciences, Charles Perkins Centre, Faculty of Medicine and Health, University of Sydney, Camperdown, NSW 2006, Australia. [6]Patrick G Johnston Centre for Cancer Research, Queen's University, Belfast, UK. [7]Nuffield Department of Surgical Sciences, University of Oxford, Oxford, UK. ✉email: zeyad.nassar@adelaide.edu.au; lisa.butler@adelaide.edu.au

Received: 12 December 2022 Revised: 5 December 2023 Accepted: 13 December 2023
Published online: 12 January 2024

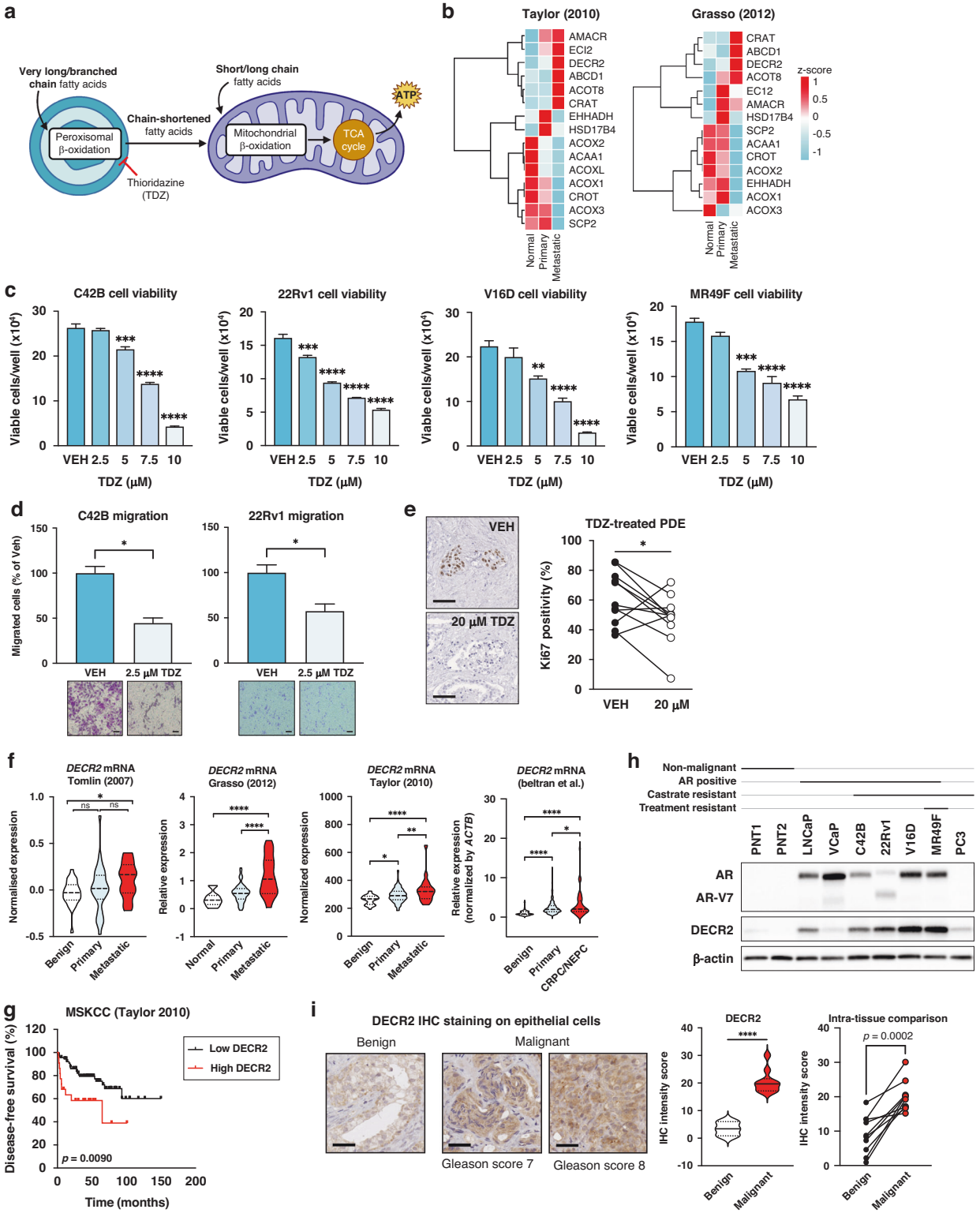

Peroxisomes are organelles that regulate the synthesis and turnover of complex lipids, including the β-oxidation of very-long chain fatty acids (VLCFA) (Fig. 1a), synthesis of bile acids and ether lipids (such as plasmalogens), α-oxidation of branched-chain fatty acids (BCFA), and regulate cholesterol biosynthesis. Although both the peroxisome and mitochondria share similar functions (for example, both organelles can degrade fatty acids and produce/scavenge reactive oxygen species), it is becoming increasingly clear that peroxisomes are indispensable organelles that are essential for cellular well-being. For instance, peroxisomes are the sole organelles in humans able to break down VLCFAs and the only ones performing α-oxidation. Despite the critical roles of peroxisomes in lipid metabolism, the functional effects of peroxisomal β-oxidation (perFAO) in cancer are not well recognised and not as intensively studied as those of mitochondria. To this end, the most well-characterised perFAO enzyme in PCa is α-methylacyl-CoA racemase

Fig. 1 DECR2 is overexpressed in prostate cancer. a Illustration of fatty acid oxidation in the peroxisome and mitochondria. Thioridazine (TDZ) is an inhibitor of perFAO. **b** Heatmap of peroxisomal β-oxidation (perFAO) gene expression in Taylor and Grasso cohorts. We manually curated a list of perFAO genes based on Gene Ontology pathway. Cell viability of (**c**) castrate-resistant C42B, 22Rv1 and V16D, and enzalutamide-resistant MR49F prostate cancer cell lines across a range of TDZ doses. **d** C42B and 22Rv1 prostate cancer cell lines treated with 2.5 μM TDZ were assessed for cell migration using transwell migration assay. Scale bar: left, 100 μm; right, 200 μm. **e** Immunostaining for proliferative marker Ki67 in vehicle (VEH) or TDZ-treated (20 μM) patient-derived explants (PDEs). Immunohistochemical staining and quantification of the proliferative marker Ki67 is shown ($n = 11$). Scale bar, 50 μm. **f** DECR2 expression with respect to tumour progression in four independent datasets. DECR2 levels were analysed in normal, primary, and metastatic castrate-resistant or neuroendocrine tissue samples. **g** The association of DECR2 expression and disease-free survival in the MSKCC (Taylor) cohort. **h** DECR2 protein expression in non-malignant prostate cell lines (PNT1 and PNT2) and prostate cancer cell lines (LNCaP, VCaP, C42B, 22Rv1, V16D, PC3), including enzalutamide-resistant prostate cancer cell line (MR49F). **i** *Left*: Representative DECR2 IHC staining of benign prostate tissues and prostate cancer tissues. Scale bar, 50 μm. *Middle*: DECR2 protein expression in a validation cohort consisting of benign prostate tissues ($n = 3$) and prostate cancer tissues ($n = 10$). *Right*: Intra-tissue IHC analysis of DECR2 expression in prostate cancer tissues ($n = 10$). All cell line data are representative of at least two independent experiments and presented as mean ± s.e.m of triplicate wells. Statistical analysis was performed using ordinary one-way ANOVA or two-tailed student's *t* test. Data in (**e**) were statistically analysed using paired t-test. Data in (**g**) were statistically analysed using a two-sided log-rank test. *$p < 0.05$, **$p < 0.01$, ***$p < 0.001$ and ****$p < 0.0001$.

(AMACR; involved in β-oxidation of BCFA). AMACR is consistently overexpressed in PCa and is associated with increased PCa risk [9]. More importantly, AMACR is highly specific for PCa and thus has been employed as a PCa-specific biomarker [10]. In a more recent study, Itkonen et al. reported that peroxisomal enoyl-CoA delta isomerase 2 (ECI2; involved in β-oxidation of unsaturated fatty acids) was significantly upregulated in human PCa and is associated with poor overall patient survival [11]. Herein, we demonstrate the therapeutic efficacy of targeting perFAO in vitro and in our patient-derived prostate tumour explants (PDE) to provide the first clinically relevant evidence for targeting perFAO in PCa. We subsequently identified DECR2 as robustly overexpressed in advanced and metastatic PCa tissues and uncovered its function as a regulator of cell cycle progression and lipid metabolism. Finally, we provide evidence for a role of DECR2 and perFAO in treatment resistance, indicating a novel therapeutic vulnerability for CRPC.

MATERIALS AND METHODS

Cell lines and tissue culture

Human immortalised normal prostate epithelial cell lines PNT1 and PNT2 were obtained from the European Collection of Authenticated Cell Cultures (ECACC). Prostate carcinoma cells LNCaP and 22RV1 were obtained from the American Type Culture Collection (ATCC; Rockville, MD, USA). Castrate-resistant V16D and enzalutamide-resistant MR49F cell lines were derived through serial xenograft passage of LNCaP cells [12] and were a kind gift from Professor Amina Zoubeidi's laboratory (Vancouver Prostate Centre, Vancouver, Canada). All cell lines were verified in 2022 via short tandem repeat profiling (Cell Bank Australia). Cells were cultured in RPMI-1640 medium containing 10% foetal bovine serum (FBS; Sigma-Aldrich, NSW, Australia) in a 5% CO_2 humidified atmosphere at 37 °C; 10 μM enzalutamide was supplemented in the media for growth of MR49F cells. Thioridazine hydrochloride was purchased from Toronto Research Chemicals (Toronto, Canada) and a stock solution of 10 mM was prepared in DMSO.

Ex vivo culture of human prostate tumours

Patient-derived-explant (PDE) culture was carried out according to techniques established in our laboratory, as described previously [8]. Briefly, tissue pieces (1 mm^3) were cultured on Gelfoam sponges in 24-well plates pre-soaked in 500 μL RPMI-1640 medium supplemented with 10% FBS and antibiotic/antimycotic solution. TDZ (10 or 20 μM) was added into each well and the tissues were cultured in 5% CO_2 in humidified atmosphere at 37 °C for 48 h, then snap frozen in liquid nitrogen and stored at −80 °C, or formalin-fixed and paraffin-embedded. Clinicopathological features of the patients included in this study are shown in Supplementary Table 1.

Immunohistochemistry (IHC)

Paraffin-embedded tissue sections (2–4 μm) were prepared prior to staining as previously described. IHC staining was performed using DECR2 (ab153849 Abcam, diluted 1:1000) antibody and the 3,3′-Diaminobenzidine (DAB) Enhanced Liquid Substrate System tetrahydrochloride (Sigma Aldrich) as described previously. DECR2 staining intensity was measured by Video Image Analysis.

Analysis of publicly available prostate cancer datasets

Gene expression data were downloaded from The Cancer Genome Atlas (TCGA) data portal, cBioPortal (SU2C and MSKCC) [13], and the GEO website; Taylor et al. GSE21034 [14]; Grasso et al. GSE35988 [15]; Tomlin et al. GSE6099 [16]. Proteomics data [17] (raw MaxQuant files) was downloaded from the ProteomeXchange Consortium via the PRIDE partner repository using the dataset identifier PXD016836 and analysed independently using the R software version 3.6.3.

Western blotting

Protein lysates were collected in RIPA lysis buffer (10 mM Tris, 150 mM NaCl, 1 mM EDTA, 1% Triton X-100, 10% protease inhibitor). Western blotting on whole-cell protein lysates was performed as previously described [8]. Primary antibodies are shown in Supplementary Table 2.

Quantitative real-time PCR (qPCR)

Total RNA was extracted from cells using the RNAeasy RNA extraction kit (Qiagen), followed by cDNA synthesis using the iScript cDNA Synthesis kit (Bio-Rad) on the CFX384 Real-Time System (Bio-Rad, NSW, Australia). qPCR was performed in triplicate as previously described [8]. Relative gene expression was determined using the comparative Ct method and normalised to the internal housekeeping genes *GUSB* and *L19*. Primer sequences are shown in Supplementary Table 3.

siRNA transfection

Human DECR2 ON-TARGET plus SMART pool (L-009627-00-0005) small interfering RNAs (siRNAs) and control siRNA (D-001810-01-20 ON-TARGET plus non-targeting siRNA #1) were purchased from Millennium Science (Victoria, Australia). siRNAs (5 nM) were reverse transfected using Lipofectamine RNAiMAX transfection reagent (Invitrogen, Victoria, Australia) according to manufacturer's instructions.

Generation of inducible shDECR2 and hDECR2 LNCaP cells

For DECR2 knockdown, LNCaP cells were transduced with the non-targeting shRNA control lentiviral particles shControl (RFP-Puro) and DECR2 shRNA inducible lentiviral particles (shDECR2, RFP-Puro) designed by Horizon Discovery (Cambridge, UK). For DECR2 overexpression, LNCaP cells were transduced with empty vector lentiviral particles hControl (GFP-Puro) and hDECR2 (GFP-Puro) designed by GenTarget Inc (San Diego, CA, USA) according to manufacturer's instructions. DECR2 shRNA and hRNA sequences are provided in Supplementary Table 4.

Functional assays

Cell viability. Cells were seeded in triplicate in 24-well plates at a density of 2.5×10^4–6.0×10^4 cells/well and reverse transfected with siRNA overnight or treated with drug supplemented medium. Cells were manually counted using a hemocytometer 96 h post-siRNA knockdown or treatment and cell viability was assessed by Trypan Blue exclusion as described previously [8].

Cell proliferation/growth. Cells were seeded in 96-well plates at a density of 3×10^3–5×10^3 cells/well and treated with drug supplemented medium. Plates were then placed in the IncuCyte® live-cell analysis system (Sartorius)

and images of the cells were recorded every 6 h. Cell growth or proliferation were determined as a measure of confluency using the confluence image mask on the Incucyte® Base Analysis Software.

Cell migration. Transwell migration assays were performed using 24-well polycarbonate Transwell inserts (3422, Sigma-Aldrich). C42B and 22RV1 cells transfected overnight with siRNA were seeded into the upper chamber of the Transwell at a density of 9.0×10^4–1.5×10^5 cells/well in serum-free medium. 650 µL of medium containing 10% FBS was added to the bottom chamber. Cells were incubated at 37 °C for 48 h. For TDZ treatment, medium in both the upper and lower chambers were supplemented with TDZ (2.5 µM). Inserts were washed with PBS and non-migrated cells were gently removed using a cotton-tipped swab. The inserts were then fixed in 4% paraformaldehyde for 20 min and stained with 1% crystal violet for 30 min. Images of migrated cells were captured using the Axio Scope A1 Fluorescent Microscope (Zeiss) at 40× magnification. The number of migrated cells was counted manually and presented as percentages relative to control cells ± SEM.

Colony formation assay. DECR2 stable knockdown (shDECR2) cells or DECR2 overexpression (hDECR2) cells were prepared in a single-cell suspension before seeding in six-well plates at a density of 500 cells/well. For TDZ treatment, C42B, V16D and MR49F cells were seeded overnight and gently treated with drug-supplemented medium. Cells were incubated for 2 weeks at 37 °C with medium being replenished every 3−5 days. After 2 weeks, cells were washed with PBS and fixed with 4% paraformaldehyde, then stained with 1% crystal violet for 30 min. Colonies were counted manually and results were reported as number of colonies ± SEM.

3D Spheroid growth assay. For TDZ treatment, 22Rv1, V16D and MR49F cells were seeded (400–700 cells/well) overnight in Nunclon Sphera 96-well U-shaped-bottom microplates (Thermo Fisher) and gently treated with drug-supplemented medium. Cells were incubated for 6 days at 37 °C. Images of spheroids were captured, and the sphere volume was determined using ImageJ and the ReViSP software [18].

Flow cytometry

Cell cycle analysis. Cells were seeded in triplicate in six-well plates at a density of 3×10^5–6×10^5 cells/well and reverse transfected with siRNA overnight or treated with drug supplemented medium. Cells were collected into fluorescence-activated cell sorting (FACS) tubes and centrifuged at 1,500 rpm for 5 min, then fixed in cold 70% ethanol for 2 h. Samples were stained with 50 µg/mL of propidium iodide (PI, Sigma-Aldrich) and 100 µg/mL Ribonuclease A from bovine pancreas (Sigma-Aldrich) for 30 min at room temperature. Cells were analysed using a BD LSRFortessa X-20 Flow Cytometer (BD Biosciences). Data were evaluated using FlowJo version 10.

Apoptosis assay. Cells were seeded in triplicate in six-well plates at a density of 3×10^5–6×10^5 cells/well and reverse transfected with siRNA overnight or treated with drug supplemented medium. Cells were collected into FACS tubes and centrifuged at 1500 rpm for 5 min, then resuspended in FACS Binding Buffer (94% Hank's Balanced Salt Solution, 1% HEPES, 5% $CaCl_2$), 7-AAD (Thermo Fisher Scientific) and Annexin-V PE (BD) for 30 min in the dark. Cells were analysed using a BD LSRFortessa X-20 Flow Cytometer (BD Biosciences). Data were evaluated using FlowJo version 10.

Neutral lipid content quantification. Cells were seeded in triplicate in 24-well plates at a density of 3×10^5–6×10^5 cells/well and reverse transfected with siRNA overnight or treated with drug supplemented medium. Cells were collected into FACS tubes and centrifuged at 1,500 rpm for 5 min, then resuspended in 2 µM of fluorescent neutral lipid dye BODIPY 493/503 (Thermo Fisher Scientific) for 15 min at 37 °C. Cells were resuspended in 300 µL FACS Binding Buffer and analysed using a BD LSRFortessa X-20 Flow Cytometer (BD Biosciences). Data were evaluated using FlowJo version 10.

LIPIDOMICS

Lipid extraction, mass spectrometry, and data analysis methods were performed as previously described [8]. Unpaired t-test *p* values and FDR-corrected *p* values (using the Benjamini/Hochberg procedure) were calculated using R version 4.1.2 and visualised using ggplot2 version 3.3.5.

RNAseq

RNA extraction and library preparation. For RNAseq, six biological replicates of V16D and MR49F prostate cancer cells subjected to either siControl or siDECR2 knockdown for 72 h were analysed. Total RNA was extracted using TRIzol reagent (Thermo Fisher) and the RNeasy Micro Kit (Qiagen) and then depleted for DNA using RNase-Free DNase Set (Qiagen). RNA quality and quantity were determined using the Tapestation 2200 and Qubit, respectively. Libraries were generated using the Nugen Universal Plus mRNA-seq protocol and converted to MGI-compatible libraries using the MGIEasy Universal Library Conversion Kit. Libraries were sequenced on the MGI DNBSEQ G400 (paired-end reads, 2×98 bp) at the South Australian Genomics Centre (SAGC), South Australian Health and Medical Research Institute, Australia.

RNAseq analysis. Sequence read quality was assessed using FastQC version 0.11.3 and trimmed with Trimmomatic version 0.36 with a sliding window of a minimum PHRED score of 20 and a window size of 4 nucleotides. Reads were also filtered for a minimum length of 36 nucleotides. Next, reads were aligned to GRCh38 human genome with Ensembl version 105 annotation using STAR version 2.7.9a. Gene count matrix was generated with FeatureCounts version subread-2.0.3. Count matrix were imported into R version 4.1.2 for further analysis and visualisation using ggplot2 version 3.3.5. Counts were normalised using the trimmed mean of M values (TMM) method in EdgeR version 3.36 and represented as counts per million (cpm). Differential gene expression analysis was performed using the glmLRT function in EdgeR. Genes with <2 cpm in at least 25% of samples were excluded from the differential expression analysis. Gene Set Enrichment Analysis (GSEA) was carried out using the GSEA software version 4.2.2 and the Molecular Signatures Database (MSigDB) to identify Hallmark and GO biological processes/pathways that were differentially regulated in the absence of DECR2. Data from GSEA were visualised using the Enrichment Map plugin [19] in Cytoscape version 3.9.1 to generate the gene interaction network. The resulting network map was filtered using FDR < 0.01 and curated to remove redundant and uninformative nodes, resulting in a simplified network. The RNA sequencing data has been deposited with Gene Expression Omnibus, with accession number GSE218282.

Metabolomics: acyl-carnitine measurement

For TDZ treatment. V16D cells were treated with varying doses of TDZ for 48 h in six-well plates. Metabolite extraction was performed as previously described [8].

For DECR2 knockdown. Acyl-carnitines were measured by LCMS, using a Thermo Scientific Q-Exactive-HF-X Hybrid Quadrupole Orbitrap system. V16D cells subjected to siControl or siDECR2 knockdown for 96 h supplemented with 100 µM DHA were washed in ice-cold isotonic NaCl and lysed in 600 µL 1:1 methanol:water. 600 µL chloroform containing the internal standard d3-palmitoyl carnitine was added to the cell slurry to induce phase separation. The organic phase was dried by speedvac, resuspended in 100 µL 4:2:1 (v/v) isopropanol:methanol:chloroform containing 7.5 mM ammonium formate, and transferred into HPLC vials. Analyte separation was achieved using an Agilent Poroshell 120, EC-C18, 2.1 × 150 mm, 2.7 µm column. The pair of buffers used were 60:40 acetonitrile:water (v/v) with 10 mM ammonium formate and 0.1% formic acid (mobile phase A), and 90:10 isopropanol:acetonitrile (v/v) with 10 mM ammonium formate and 0.1% formic acid (mobile phase B), flowed at 200 mL/min and in positive mode. MS1 data was acquired with the following settings: 3.5 kV, capillarity temperature at 300 °C, resolution 120,000, injection time 100 ms, AGC 1×10^6, scan range 200–500. For ddMS2 data acquirement, the following settings were used: top 10, resolution 30,000, 200–2000, isolation 1.0 m/z, nce 30, AGC target 1×10^3, intensity threshold 5×10^4, dynamic exclusion 20 s. Acyl-carnitine peak areas were identified

and extracted using MS-Dial and were normalised to the internal standard.

In vivo studies

Orthotopic tumour growth (shDECR2). 10 µL containing 1×10^6 DECR2 inducible knockdown cells (shDECR2) were injected intraprostatically in 8-week-old NOD scid gamma (NSG) male mice. Whole-body imaging to monitor luciferase-expressing LNCaP cells was performed on day 3 of the injection and once weekly after that using the In Vivo Imaging System (IVIS, PerkinElmer). Following 1-week post-injection, mice were randomised into two groups: Group A (shDECR2-dox) mice were fed with sucralose-containing water (25 mM); Group B (shDECR2+dox) mice were fed with doxycycline/sucralose-treated water (2 mg/mL). D-luciferin (potassium salt, PerkinElmer) was dissolved in sterile deionised water (0.03 g/mL) and injected subcutaneously (3 mg/20 g of mouse body weight) before imaging. Bioluminescence is reported as the sum of detected photons per second from a constant region of interest. After the animals were sacrificed, lungs and livers were excised for ex vivo imaging using the IVIS system.

Orthotopic tumour growth (hDECR2). 10 µL containing 1×10^6 DECR2 overexpression cells (hDECR2) or negative control cells (hControl) were injected intraprostatically in 8-week-old NSG male mice. Whole-body imaging to monitor luciferase-expressing LNCaP cells was performed at day 3 of the injection and once weekly after that using the In Vivo Imaging System (IVIS, PerkinElmer). D-luciferin (potassium salt, PerkinElmer) was dissolved in sterile deionised water (0.03 g/mL) and injected subcutaneously (3 mg/20 g of mouse body weight) before imaging. Bioluminescence is reported as the sum of detected photons per second from a constant region of interest. After the animals were sacrificed, lungs and livers were excised for ex vivo imaging using the IVIS system.

After each study, tumours that were excised were snap frozen for RNA extraction and formalin-fixed and paraffin-embedded.

Statistical analysis. Results are reported as mean ± SEM. Statistical analysis was performed using GraphPad Prism (V9.0 for Mac). The differences between treatment groups were compared by t-test or one-way ANOVA followed by Tukey or Dunnett post hoc test, unless otherwise stated in the figure legends. Significance is expressed as $*p < 0.05$, $**p < 0.01$, $***p < 0.001$, $****p < 0.0001$.

RESULTS

The peroxisomal β-oxidation enzyme, DECR2, is overexpressed in prostate cancer

Little is known about targeting the enzymes of perFAO or their expression in PCa. Accordingly, we evaluated the expression of a set of peroxisome-related genes (obtained from the KEGG database) in the Taylor cohort [14] composed of primary ($n = 131$) and metastatic ($n = 19$) tumour tissues and noticed a significant variation in the expression of these genes with tumour progression (Supplementary Fig. 1a). Next, we focused on genes that are involved in perFAO by interrogating GO terms (Molecular Signatures Database, MSigDB) for perFAO, manually curating a list of $n = 15$ genes that were involved in perFAO, and examining their expression in the Taylor and Grasso [15] (primary $n = 59$, metastatic CRPC $n = 35$) cohorts (Fig. 1b). Despite variability in their expression, this approach revealed several perFAO genes: *ECI2, DECR2, ABCD1, CRAT*, and *ACOT8* (Fig. 1b) involved in regulation of fatty acid metabolism and energy homoeostasis that were consistently upregulated in both cohorts in metastatic tissues, suggesting an important role for perFAO in PCa.

We next evaluated the efficacy of targeting perFAO using a potential clinical candidate agent and inhibitor of perFAO, thioridazine (TDZ) [20, 21], in CRPC and treatment-resistant PCa cells (Fig. 1a). TDZ is a first-generation antipsychotic drug that was withdrawn from the global market in 2005 due to a well-defined risk of cardiac arrythmias. Nevertheless, TDZ continues to be used off-label for patients with severe or chronic schizophrenia who are refractory to other treatment options [22]. In recent years, TDZ has been increasingly used as a perFAO inhibitor [21, 23], likely through its inhibitory effects on Cytochrome P450 enzymes [21]. TDZ induced a dose-dependent reduction in cell viability of CRPC cells (C42B, 22Rv1, V16D cell lines) and acquired ENZ-resistant MR49F cells (Fig. 1c). Furthermore, we tested the ability of TDZ to impede cell migration of C42B and 22Rv1 CRPC cells and showed significantly reduced migration at a low dose of 2.5 µM of TDZ (Fig. 1d). TDZ significantly and dose-dependently decreased colony formation ability, and induced apoptosis and cell death in CRPC C42B, V16D and ENZ-resistant MR49F cell lines (Supplementary Fig. 1b, c). Our recent report demonstrated the efficacy of targeting mitochondrial β-oxidation using the chemical inhibitor, etomoxir [8], using our well-defined patient-derived explant (PDE) model that recapitulates the complexity of the clinical tumour microenvironment [24]. Herein, we evaluated the clinical efficacy of targeting perFAO using 20 µM TDZ in PDE tissues and observed an overall significant reduction in cell proliferation, with only three patients showing no antiproliferative response (Fig. 1e). Although not significant, a lower dose of 10 µM TDZ demonstrated an overall modest anti-proliferative activity in PDE tissues, with 6 out of 11 patients showing a treatment-related decrease in proliferation (Supplementary Fig. 1e).

Our results demonstrated that TDZ is efficacious in vitro and ex vivo and provide proof-of-concept that targeting perFAO may be a promising therapeutic strategy. However, no specific inhibitors of perFAO currently exist. In view of our recent discovery of the role of mitochondrial DECR1 in PCa [8] and its upregulation in metastatic tissues, we focused our attention on DECR2 as a key enzyme involved in perFAO. We further validated the overexpression of DECR2 mRNA in the Tomlin [16] ($n = 51$ primary and metastatic PCa) and Beltran [25] (CRPC $n = 34$, neuroendocrine PCa $n = 15$) cohorts and observed significantly higher levels of DECR2 in metastatic tissue compared with primary (Beltran cohort) or normal tissue (Tomlin and Beltran cohorts) (Fig. 1f). In line with this observation, DECR2 gene copy number gain was evident in several clinical PCa datasets (acquired from cBioportal; Supplementary Fig. 1d). Higher DECR2 levels were also significantly associated with biochemical recurrence in the MSKCC (metastatic CRPC) cohort (Fig. 1g). Next, we examined DECR2 protein expression in a panel of PCa cell lines: DECR2 levels were low in AR-positive, androgen-dependent LNCaP cells and AR-positive CRPC C42B cells, intermediate in AR-positive CRPC 22Rv1 cells, and high in AR-positive CRPC V16D and ENZ-resistant MR49F cell lines (Fig. 1h). Similarly to publicly available datasets, we also observed an increase in DECR2 expression in malignant PCa tissues ($n = 10$) compared with benign tissues ($n = 3$), as assessed using quantitative immunohistochemistry staining analysis. Notably, intra-tissue analysis revealed a significant increase in DECR2 expression in malignant regions versus benign regions within the same tissue core (Fig. 1i, Supplementary Fig. 1e). Consistent with its known function, we confirmed DECR2 localisation in the peroxisome using immunocytochemistry (Supplementary Fig. 1g). Furthermore, we provide evidence supporting the perFAO selectivity of TDZ by demonstrating that overexpression of DECR2 markedly increased susceptibility of LNCaP cells to TDZ treatment, while TDZ had no effect on DECR2 knockdown cells (Supplementary Fig. 1h, i). Finally, we showed that DECR2 knockdown and TDZ treatment inhibited perFAO in V16D cells, as demonstrated by the significant accumulation of multiple acylcarnitine species after supplementation with docosahexaenoic acid (DHA; very long chain fatty acid) (Supplementary Fig. 1j, k).

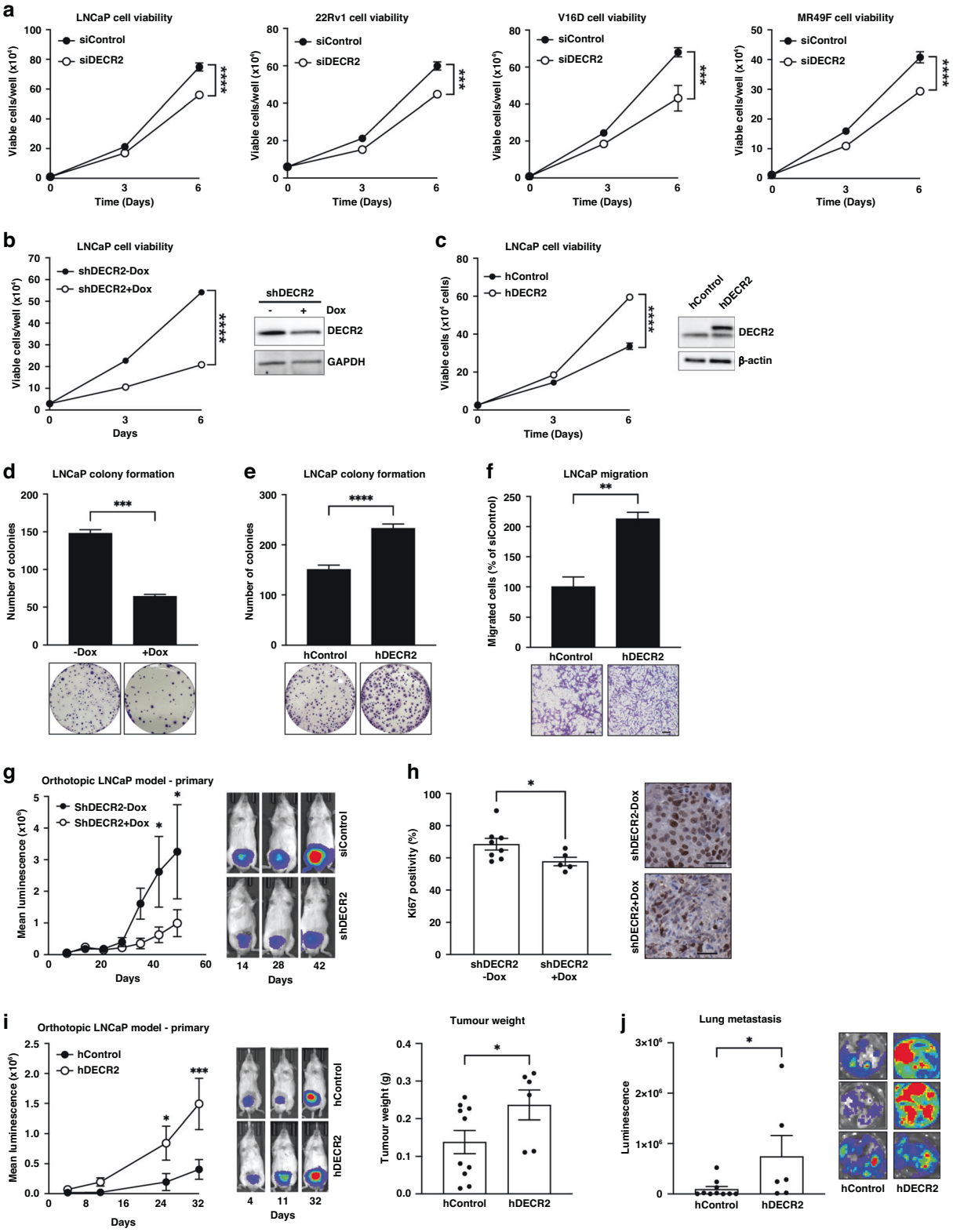

DECR2 targeting inhibits prostate cancer oncogenesis

The upregulation of DECR2 levels in metastatic CRPC compared to benign tissues suggests an important role for DECR2 in PCa growth and progression. Indeed, transient knockdown of DECR2 significantly suppressed viability and induced cell death in androgen-dependent LNCaP, CRPC 22Rv1 and V16D, and enzalutamide-resistant MR49F PCa cell lines (Fig. 2a, Supplementary Fig. 2a). Notably, no effect on cell viability was observed in non-malignant PNT1 prostate cells (Supplementary Fig. 2b). Similarly, doxycycline (dox)-inducible knockdown of DECR2 with short hairpin RNA (shDECR2+Dox) significantly attenuated viability in LNCaP and 22Rv1 PCa cell lines (Fig. 2b; Supplementary Fig. 2d), but no effect was observed in dox-inducible control (shControl+Dox) cells (Supplementary Fig. 2c, d). In contrast, constitutive ectopic overexpression of DECR2 (hDECR2) in

Fig. 2 DECR2 knockdown inhibits prostate cancer cell growth in vitro and in vivo. a Cell viability of androgen-dependent LNCaP, castrate-resistant 22Rv1 and V16D, and enzalutamide-resistant MR49F prostate cancer cell lines subjected to siRNA-mediated DECR2 knockdown. **b** Cell viability of LNCaP cells with stable/inducible shRNA DECR2 knockdown (shDECR2) and (**c**) stable overexpression of DECR2 (hDECR2). **d** LNCaP colony formation was evaluated in cells with stable/inducible shRNA DECR2 knockdown (shDECR2) or (**e**) stable DECR2 overexpression (hDECR2). **f** LNCaP stable DECR2 overexpression (hDECR2) cell lines were assessed for cell migration using a transwell migration assay. Scale bar, 100 µm. **g** LNCaP cells with stable/inducible shRNA knockdown of DECR2 (shDECR2+dox, $n = 11$) or control (shDECR2-dox $n = 10$) were analysed for orthotopic LNCaP tumour growth in mice, representative bioluminescent tumour images (right). **h** Ki67 quantification (left) and representative IHC staining (right) of orthotopic LNCaP tumours. Scale bar, 100 µm. This panel includes data from mice with sufficient sized tumours for analysis (shDECR2+dox $n = 5$, shDECR2-dox $n = 8$). Scale bar, 50 µm. **i** Tumour growth and tumour weight of intraprostatically injected LNCaP cells with stable DECR2 overexpression (hDECR2, $n = 6$) or control (hControl, $n = 10$), representative bioluminescent tumour images (right). **j** Lung luminescence readings of stable DECR2 overexpression tumours in mice. All in vitro data are representative of at least two independent experiments and presented as mean ± s.e.m of triplicate wells. Statistical analysis was performed using ordinary one-way ANOVA or two-tailed student's t-test: *$p < 0.05$, **$p < 0.01$, ***$p < 0.001$ and ****$p < 0.0001$.

LNCaP cells significantly enhanced viability compared with vector control cells (hControl; Fig. 2c). Additionally, dox-inducible knockdown of DECR2 markedly decreased LNCaP and 22Rv1 colony formation (Fig. 2d; Supplementary Fig. 2e, f) while stable overexpression of DECR2 increased colony formation (Fig. 2e). Likewise, DECR2 knockdown significantly reduced migration of CRPC C42B and 22Rv1 PCa cells (Supplementary Fig. 2g), while stable overexpression of DECR2 increased migration in LNCaP cells (Fig. 2f). Finally, dox-induced shDECR2 (shDECR2+Dox) cells showed significantly reduced capacity for tumour growth, with luminescence readings positively correlated with final tumour weights, and a trend towards reduced lung metastasis compared with non-dox-induced (shDECR2-Dox) cells using LNCaP orthotopic xenografts (Fig. 2g; Supplementary Fig. 2h). Inspection of the tumours also revealed significantly reduced cellular proliferation in shDECR2+Dox cells compared with shDECR2-Dox cells (Fig. 2h). In contrast, overexpression of DECR2 in LNCaP cells significantly increased tumour growth compared with control cells (Fig. 2i, Supplementary Fig. 2i). In addition, analysis of detectable tumours from hDECR2 ($n = 6$) and hControl ($n = 10$) mice revealed a significant increase in tumour weight and lung metastasis of hDECR2 cells compared with control cells (Fig. 2i, j).

Depletion of DECR2 induces cell cycle arrest

To investigate the mechanism by which PCa cell growth and proliferation was attenuated by knockdown of DECR2, we carried out genome-wide transcriptional profiling of V16D and MR49F PCa cells ($n = 6$ biological replicates for each) subjected to a pooled siRNA-mediated knockdown of DECR2 (Fig. 3a). Differential expression analysis identified >8000 genes that were significantly (FDR < 0.05) differentially expressed in DECR2 knockdown cells compared to control cells (Supplementary Data 1). Gene Set Enrichment Analysis (GSEA) revealed a strong enrichment for GO-terms/pathways (MSigDB) related to the cell cycle and DNA replication and repair processes among downregulated genes in DECR2 knockdown cells compared with control cells (Supplementary Data 1). Other metabolic processes such as carboxylic acid pathways, branched-chain amino acid and isoprenoid metabolic processes were enriched among genes upregulated in DECR2 knockdown cells (Fig. 3b; Supplementary Fig. 3a**;** Supplementary Data 1). GSEA analysis of the Hallmark pathway terms (MSigDB) identified E2F targets to be enriched among downregulated genes (Fig. 3c). Accordingly, we examined the effect of DECR2 knockdown on cell cycle profile by flow cytometry. Knockdown of DECR2 induced cell cycle arrest at the G1/S phase in V16D and MR49F PCa cell lines (Fig. 3d). Further, we validated our observations via qPCR in inducible DECR2 knockdown and overexpression cells (Supplementary Fig. 3b, c). Stable overexpression of DECR2 in LNCaP cells showed the opposite effect where there were enhanced proportions of cells in S phase, consistent with an increase in cell proliferation (Supplementary Fig. 3d). Likewise, TDZ induced G1/S phase cell cycle arrest dose-dependently in V16D and MR49F cells, particularly at the 10 µM dose (Fig. 3e). In light of these findings, we assessed the effect of DECR2 knockdown on several cell-cycle related proteins/regulators in V16D and MR49F cells. We observed an increase in cyclin-dependent kinase inhibitors p21 and p27, and a decrease in cyclin-dependent kinase CDK4 (Fig. 3f). Notably, we observed a decrease in phosphorylated retinoblastoma (pRb), a tumour suppressor protein in DECR2 knockdown cells compared to control cells (Fig. 3f). We next evaluated whether the cyclin-dependent kinase (CDK) 4/6 inhibitor, ribociclib (Rib) could further enhance the effect of DECR2 knockdown. Indeed, Rib further reduced growth of DECR2-depleted V16D and MR49F cell lines (Fig. 3g). In contrast, stable overexpression of DECR2 in LNCaP cells rendered the cells more resistant to Rib compared to control cells (Supplementary Fig. 3d, e). Finally, we examined the effect of perFAO inhibition via TDZ in combination with Rib on PCa cell viability. We found that TDZ further abrogated growth of V16D and MR49F cell lines when treated in combination with Rib compared to vehicle-treated cells or Rib alone (Fig. 3h).

One of the most strongly enriched pathways from our RNAseq data was lipid metabolism and fatty acid metabolic processes (Fig. 3b; Supplementary Fig. 3a). Consistent with these data, transcription factor enrichment analysis [26] identified several lipid metabolism-related transcription factors (i.e., HNF4G, HNF4A, PPARG) that were significantly enriched among the top upregulated differentially expressed genes in DECR2 knockdown cells (Supplementary Fig. 3f).

DECR2 depletion dysregulates lipid metabolism of prostate cancer cells

Given the biological role of DECR2 in perFAO, and the enrichment for lipid metabolic pathways in DECR2-depleted cells above, we further explored the impact of perturbing DECR2 on lipid metabolism. Knockdown of DECR2 in V16D and MR49F PCa cells significantly induced neutral lipid accumulation, suggesting storage of lipids in lipid droplets (Supplementary Fig. 4a). Likewise, TDZ dose-dependently increased neutral lipid accumulation in V16D and MR49F PCa cell lines (Supplementary Fig. 4b). To understand how cellular lipid composition is altered by DECR2 knockdown, we carried out a global lipidomic analysis of LNCaP, V16D and MR49F PCa cells subjected to siRNA-mediated knockdown of DECR2 (Fig. 4a). Inspection of the lipid profiles of LNCaP, V16D and MR49F PCa cells after transient knockdown of DECR2 revealed a profound remodelling of the cellular lipidome (Fig. 4b). All 3 cell lines displayed a strong and consistent accumulation of many cellular lipids (Fig. 4b; Supplementary Fig. 4c; Supplementary Data 2), in particular the cholesteryl esters, glycerides, sphingolipids, and several classes of (lyso)-phospholipids such as PC, PE, PI and LPE (Fig. 4b; Supplementary Fig. 4e). Interestingly, we also observed the accumulation of several classes of ether-linked phospholipids such as PC-O, PE-O and PE-P (Fig. 4b; Supplementary Fig. 4e), which are known to be synthesised within the peroxisome [27]. DECR2 knockdown did not markedly alter saturated fatty acids (SFA) levels, but significantly increased the

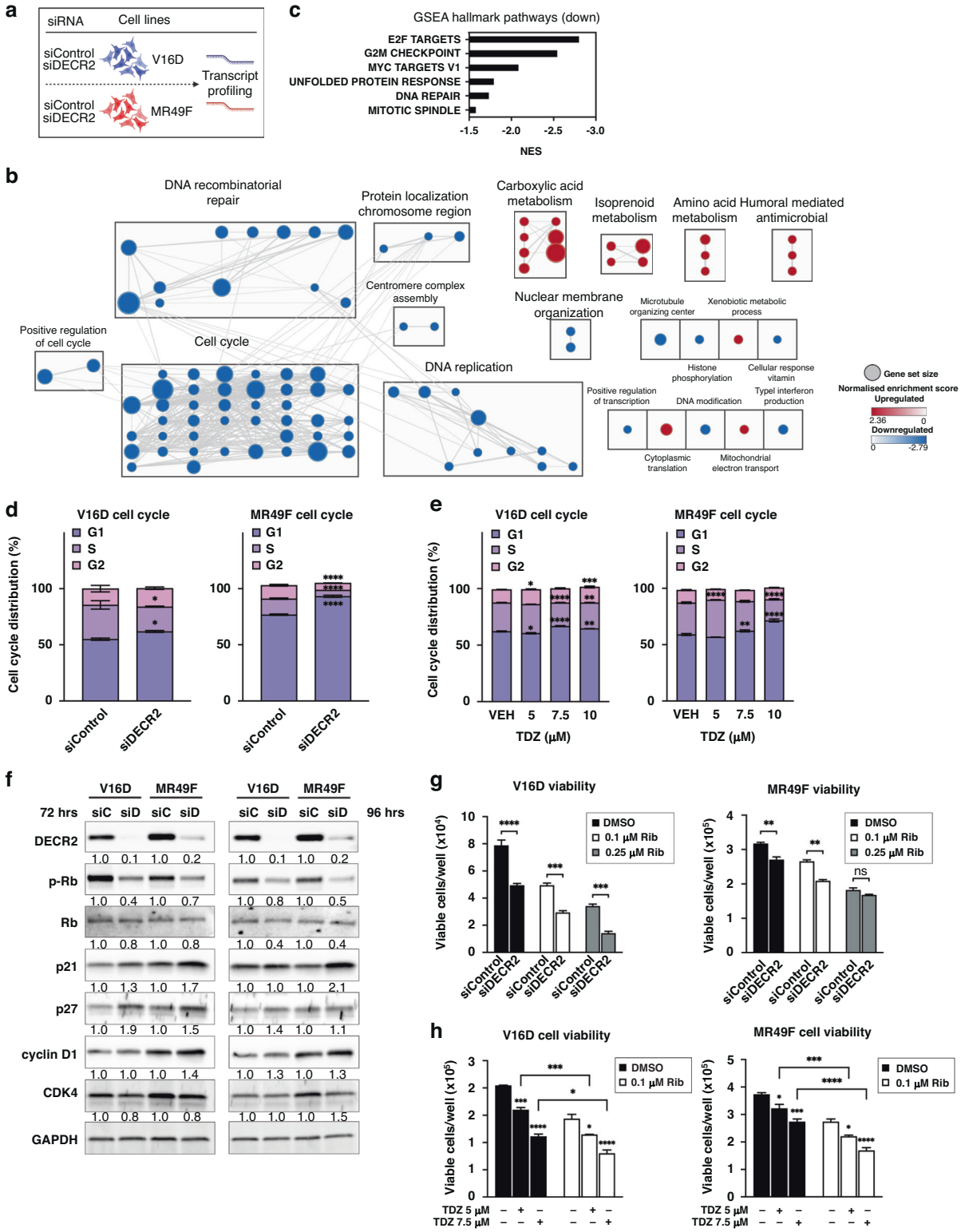

abundance of monounsaturated (MUFA) and polyunsaturated fatty acids (PUFA) compared with control cells (Fig. 4c). The opposite effect on lipid accumulation was observed in DECR2-overexpressing (hDECR2) LNCaP cells, whereby we observed a significant reduction in total lipid levels (Fig. 4d; Supplementary Fig. 4d; Supplementary Data 2). Analysis of the lipidome revealed marked decrease in abundance across almost all classes of lipids compared with control cells, except triacylglycerides (TAG) which showed a significant increase in levels (Fig. 4d; Supplementary Fig. 4f). Overexpression of DECR2 in LNCaP cells markedly decreased SFA, MUFA and PUFA abundance compared with control cells (Fig. 4e). However, closer inspection of the relative abundance revealed a significant decrease in the proportions of SFA and PUFA ($n \geq 3$) levels relative to MUFA and PUFA ($n = 2$) levels (Fig. 4f). Next, we performed a lipid ontology [28] (LION) enrichment analysis to associate lipids in DECR2 knockdown cells

Fig. 3 Transcriptomic analysis of the molecular mechanism of DECR2 function. a Schematic for DECR2-dependent RNA-seq-based changes in gene expression after DECR2 siRNA knockdown. **b** Gene interaction network of GSEA GO-terms (sourced from MSigDB, FDR < 0.01) enriched in up- (red) or down- (blue) regulated genes in DECR2 knockdown V16D and MR49F prostate cancer cells. Nodes represent gene sets and node size represents the number of genes in the gene set. Edges represent overlap between gene sets and edge width represents the number of genes that overlap (see Supplementary Data 1). **c** Bar chart of enriched GSEA Hallmark terms among downregulated genes in DECR2 knockdown cells. V16D and MR49F cell cycle distribution 96 h after (**d**) siRNA-mediated DECR2 knockdown, and (**e**) TDZ treatment. Data presented as percentage of cells in G1, S or G2 phase per sample. **f** Western blot analysis of a panel cell cycle-related protein markers in V16D and MR49F cells 72 and 96 h after DECR2 knockdown. GAPDH was used as loading control. Cell viability of (**g**) V16D and MR49F prostate cancer cells after DECR2 knockdown. **h** Cell viability of V16D and MR49F prostate cancer cells treated with TDZ (5 μM and 7.5 μM) and/or in combination with Rib (0.1 μM). All in vitro data are representative of at least two independent experiments and presented as mean ± s.e.m of triplicate wells. Statistical analysis was performed using ordinary one-way or two-way ANOVA: ns non-significant, $*p < 0.05$, $**p < 0.01$, $***p < 0.001$ and $****p < 0.0001$.

with biological features (Fig. 4g). Lipids with increased relative abundance in DECR2 knockdown samples were enriched for terms associated with lipid storage/droplet, sphingolipids, lipid-mediated signalling, PG, PI and PS, and alterations in lipids implicated in the plasma membrane and endosome/lysosome. In contrast, LION enrichment analysis revealed enrichment for terms associated with PUFAs, SM, PC, PE, plasmalogens, and membrane components such as the mitochondria and endoplasmic reticulum, among lipids downregulated in DECR2 knockdown cells.

DECR2 expression levels affect sensitivity to enzalutamide

A recent proteomics study by Blomme et al. characterised the changes associated with acquired resistance to AR pathway inhibition (ARi) [17]. Here, we independently analysed their proteomics dataset and found that MSigDB Hallmark and KEGG peroxisomal genes were strongly associated with acquired ENZ and apalutamide (APA) resistance (Fig. 5a; Supplementary Fig. 5a). Notably, DECR2 protein was robustly upregulated in ARI-resistant cells and organoids (Fig. 5b). Further, high DECR2 levels were significantly associated with overall survival ($p = 0.0233$; Fig. 5c) in the SU2C clinical PCa cohort, consisting of patients with metastatic CRPC linked to longitudinal fatal outcomes [29]. Accordingly, we assessed whether DECR2 depletion or inhibition of perFAO via TDZ could increase sensitivity of CRPC (22Rv1 and V16D) and ENZ-resistant (MR49F) PCa cells to ENZ. Indeed, DECR2 knockdown further attenuated the effects of ENZ on 22Rv1, V16D and MR49F viability (Fig. 5d) and colony formation compared to DECR2 knockdown or ENZ alone (Supplementary Fig. 5b). Similarly, we showed that TDZ in combination with ENZ further attenuated effects on 22Rv1, V16D and MR49F viability (Fig. 5e) and colony formation (Supplementary Fig. 5c) compared to TDZ or ENZ alone —most notably in the ENZ-resistant MR49F cells, suggesting re-sensitisation to ENZ (Supplementary Fig. 5c). TDZ in combination with ENZ also significantly decreased 22Rv1, V16D and MR49F growth in 3D spheroids (Fig. 5f), which better mimics in vivo conditions than 2D cell culture [30], more effectively than TDZ or ENZ alone. To investigate whether high DECR2 levels could confer resistance to ARi, we assessed cell viability of stable overexpression of DECR2 in LNCaP cells under androgen-depleted conditions. Stable overexpression of DECR2 significantly increased growth of LNCaP cells compared with vector control cells cultured in charcoal-stripped serum medium (Fig. 5g, Supplementary Fig. 5d). Next, we assessed cell viability of stable DECR2 overexpression LNCaP cells under AR inhibition via treatment with ENZ and APA. In both conditions, stable DECR2 overexpressing LNCaP cells were significantly more resistant to ARi compared to vector control cells (Fig. 5h).

DISCUSSION

Peroxisomal β-oxidation (perFAO) is an understudied aspect of fatty acid metabolism in PCa. To provide proof-of-principle of its biological importance, we initially appropriated an existing clinically available pharmacological agent to explore the efficacy and clinical exploitability of inhibiting perFAO, using thioridazine (TDZ) [20]. The anti-tumorigenic effects of TDZ have been reported in several other cancer cell types such as the brain, lung, colon, ovarian and breast [31]. In this study, we provide first-in-field evidence for the therapeutic efficacy of targeting perFAO, using TDZ, in clinical prostate tumours and in in vitro cell line models of treatment-resistant PCa. Altogether, our findings suggest that perFAO is an exploitable therapeutic target for PCa. However, recognising that TDZ is not an ideal inhibitor of perFAO due to its uncertain specificity and considering that no other perFAO inhibitors currently exist, we sought to identify key functional genes of perFAO that could be more selectively targeted therapeutically.

Cancer-related changes in peroxisomal gene and protein expression as well as metabolic flux, and their relationship to cellular lipid profile, remain an area ripe for further investigation. Various tumour types exhibit alterations in peroxisome abundance and activity, and it was recently reported that expression of peroxisomal genes is elevated across different tumours [32]. Intriguingly, while some studies have observed a decrease in peroxisomal activity in certain tumour types, other groups indicated that peroxisomal metabolic activities promote tumour growth. It is likely that the tumour-promoting or tumour-suppressing functions of peroxisomes are dependent on the tumour type and disease stage [33]. Accordingly, our analysis of the expression of genes involved in peroxisome/β-oxidation in clinical PCa revealed two distinct expression profiles that are either up- or down-regulated with increasing tumour progression.

Not surprisingly, *AMACR* was one of the most consistently upregulated perFAO genes across all stages of PCa, accompanied by *DECR2*. Notably, DECR2 protein expression was highest in castrate-resistant V16D and ENZ-resistant MR49F PCa cell lines. 2,4-dienoyl CoA reductase 2 or DECR2 is a perFAO enzyme analogous to our recently discovered mitochondrial DECR1. Besides residing in different cellular compartments, DECR1 and 2 are both critical NADPH-dependent auxiliary enzymes that play key roles in (poly)unsaturated fatty acid oxidation [34]. Unlike the mitochondria, peroxisomes do not produce ATP. Instead, peroxisomes function to shorten very long chain fatty acids (VLCFA, C ≥ 22) prior to transport into the mitochondria for complete degradation and energy production [27]. Although examination of the crystal structure of DECR2 showed selectivity for VLCFAs like docosahexaenoic acid (DHA) [35], another study reported that DECR2 may also be involved in the degradation of short and medium chain substrates [36]. In a very recent study, Spiegel et al. characterised the lipidomic changes of a set of gene knockouts, including DECR2, in a colon cancer cell line. The authors observed elevated levels of long-chain PUFAs in PI, PE-O and PC-O lipid classes (C20 and C22), confirming previous studies that DECR2 can oxidise unsaturated fatty acids and assist in the degradation of PUFAs such as arachidonic acid (AHA) and DHA in peroxisomes [37]. Accordingly, our data demonstrated that DECR2 knockdown and TDZ treatment increased the levels of several acylcarnitine species in cells supplemented with DHA, indicating inhibition of

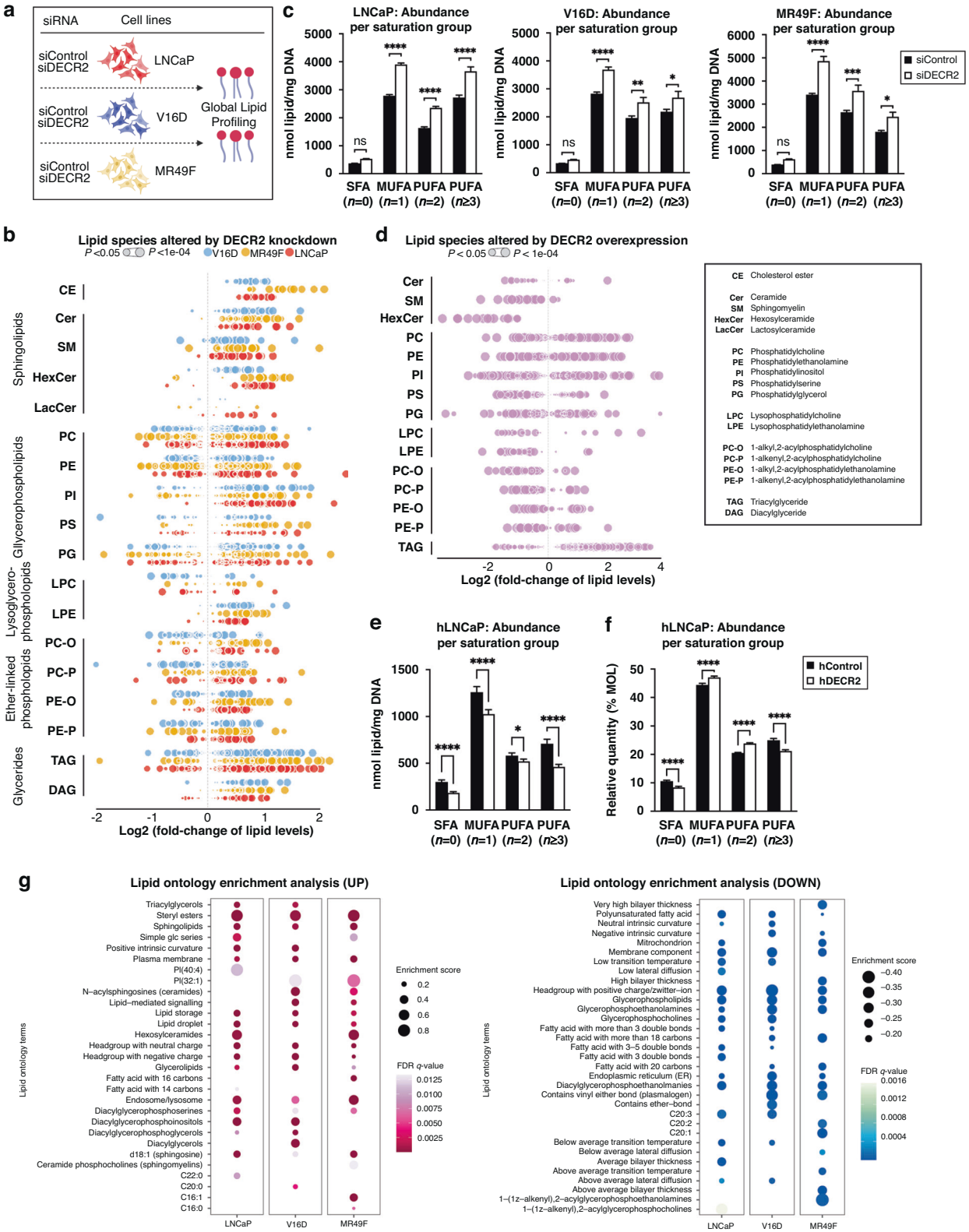

Fig. 4 Global lipidomics of DECR2 knockdown and overexpression in prostate cancer cells reveal strongly altered lipid states. a Global lipidomic study overview. **(b)** Lipidomic analysis of LNCaP, V16D and MR49F prostate cancer cell lines subjected to siRNA-mediated DECR2 knockdown relative to control. Values are shown as quantitative log2-fold changes. Lipidomics data were from 6 replicates and are represented as means. Each dot represents a lipid species. Dot size is proportionate to statistical significance (see Supplementary Data 2). **c** Quantitative abundance per saturation group in LNCaP, V16D and MR49F cells. **d** Lipidomic analysis of DECR2 overexpression (hDECR2) cells relative to control (hControl). **e** Quantitative abundance. **f** Relative abundance per saturation group in DECR2 overexpression cells. **g** Lipid ontology (LION) enrichment analysis of relative lipid abundance in siControl versus siDECR2 LNCaP, V16D and MR49F prostate cancer cells. Statistical analysis was performed using two-tailed student's *t* test: $*p < 0.05$, $**p < 0.01$, $***p < 0.001$ and $****p < 0.0001$.

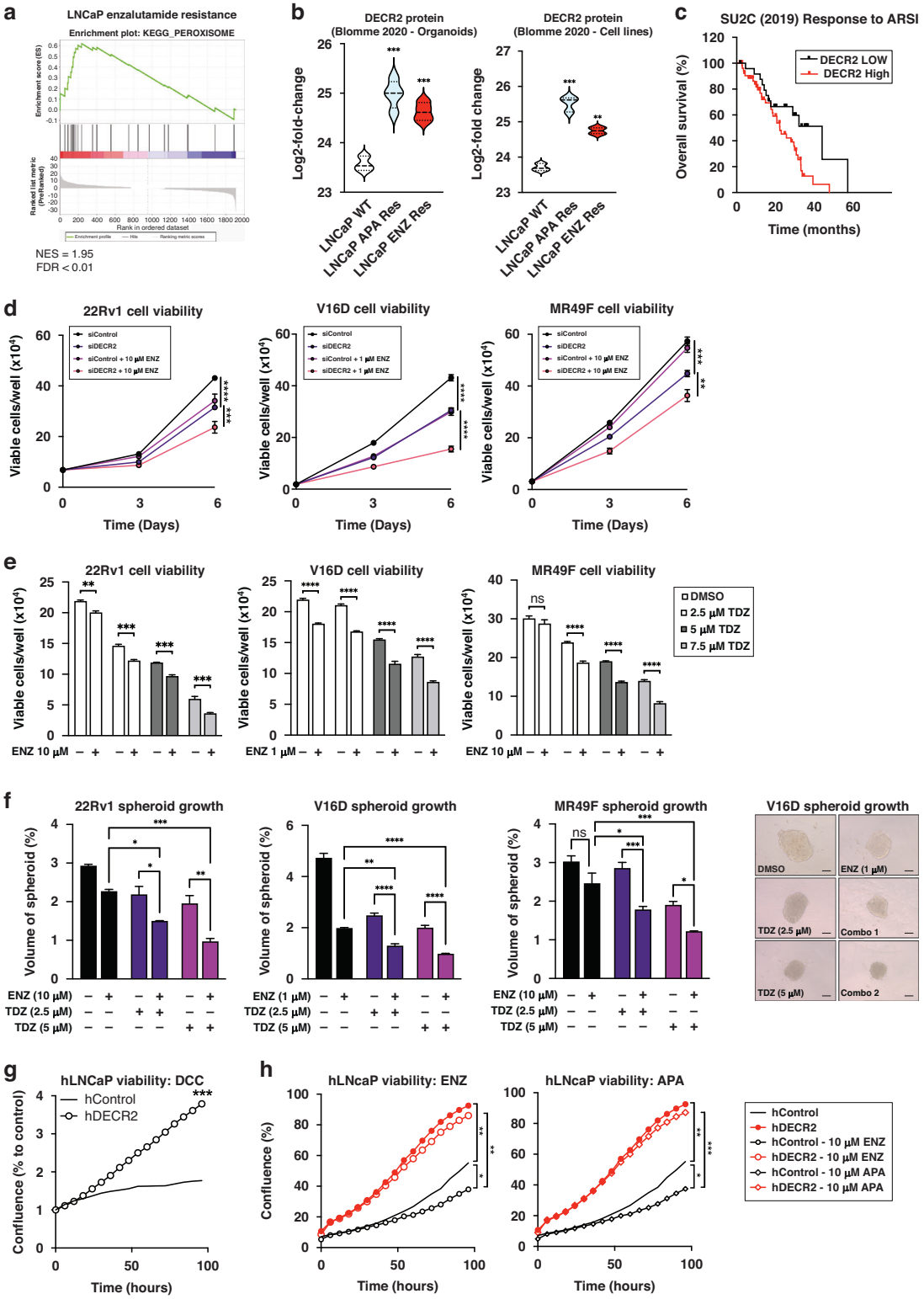

perFAO. As we cannot ascertain specific acylcarnitine species to DECR2, more work is needed to elucidate its exact fatty acid substrate.

Our findings shed new light on perFAO in regulating cell cycle progression and lipid metabolism. One of the cellular processes most markedly affected by DECR2 targeting is the cell cycle, as demonstrated by our RNAseq data. We further showed that DECR2 knockdown markedly arrested the cell cycle at the G1 phase, while high DECR2 levels exhibited an accelerated rate of cell cycle progression. Consistent with our results, we observed a decrease in phosphorylated retinoblastoma (pRb) tumour suppressor protein in DECR2 knockdown compared with control cells. Of particular interest is the connection between peroxisomal fatty acid metabolism and cell cycle progression. We observed that DECR2 knockdown or overexpression had profound effects on the cellular lipidome, notably for altered lipid abundance and composition. Koberlin et al.

Fig. 5 DECR2 confers resistance to enzalutamide in prostate cancer cells. a GSEA of peroxisomal Hallmark and KEGG proteins shows positive correlation with acquired resistance to enzalutamide. **b** DECR2 protein expression is significantly increased in LNCaP acquired apalutamide and enzalutamide resistance organoids and cell lines compared to wildtype LNCaP organoids and cells. Data are represented as violin plots in GraphPad prism. **c** The correlation of DECR2 expression with overall survival in the SU2C cohort. ARSI = androgen receptor signalling inhibitor. **d** Cell viability of 22Rv1, V16D and MR49F cells subjected to siRNA-mediated DECR2 knockdown, treated with ENZ (1 or 10 μM). **e** Cell viability of 22Rv1, V16D and MR49F prostate cancer cell lines treated with thioridazine, TDZ (2.5, 5 and 7.5 μM) and/or ENZ (1 or 10 μM). **f** 22Rv1, V16D and MR49F cell growth in 3D spheres, treated with TDZ (2.5 and 5 μM) and/or ENZ (1 or 10 μM). Spheroid volumes were determined after four days of culturing the cells in 96-well microplates; spheres were assessed using the ReViSP software. Scale bar, 100 μm. **g** Growth of hDECR2 and hControl LNCaP cells under charcoal-stripped (androgen-deprived) conditions (DCC). **h** Growth of hDECR2 and hControl LNCaP cells under full serum conditions and in response to enzalutamide (ENZ, 10 μM) and apalutamide (APA, 10 μM). The same controls were used in both graphs in (**h**). All data are representative of at least two independent experiments and presented as mean ± s.e.m of triplicate wells. Data in (**c**) were statistically analysed using a two-sided log-rank test. Statistical analysis was performed using ordinary one-way or two-way ANOVA. ns = non-significant, *$p < 0.05$, **$p < 0.01$, ***$p < 0.001$ and ****$p < 0.0001$.

showed that functional phenotypes could be predicted based on different lipid states, and are applicable to more membrane-dependent processes such as cell division, proliferation, apoptosis, and autophagy [38]. Gokcumen et al. demonstrated that cells actively regulate their lipid composition and localisation during cell division, and that specific lipids within lipid families have specific functions that contribute to signalling and structural integrity of dividing cells [39]. Notably, our LION enrichment analysis revealed dramatic changes in glycerophospholipids in DECR2 knockdown cells, which are essential building blocks for cell growth/proliferation. perFAO contributes to glycerophospholipid (GL) synthesis [40–42]. Previous studies have also shown that key phospholipids of plasma and organelle membrane, PC and PE, are differentially regulated across the cell cycle (G1/S phase) mediated by transcription factors SREBP, AKT/mTOCR1, and p53 [43]. perFAO can also alter the GL milieu to trigger actin remodelling to enable the reorganisation of the plasma membrane needed for proper receptor localisation, recruitment of signalling intermediates and changes in cell morphology required for proliferation and survival [44]. Certain lipid species such as DGs and sphingolipids (i.e. SM and Cer) can act as second messengers, and changes in the acyl-chain composition of membrane lipids such as PC are known to impact the regulation of oncogenic signalling pathways [45]. Recent work has linked Rb/pRb to the control of lipid metabolism, including but not limited to modulation of mitochondrial oxidative phosphorylation [46] and lipid remodelling (i.e. elongation and desaturation) [47]. In addition, Rb/pRb is able to cooperate with various metabolic pathways (i.e. mTORC1, SREBP, PI3K/AKT) to facilitate homoeostatic control of cellular metabolism [48].

Intriguingly, we observed a marked increase in TG levels in DECR2 knockdown cells, suggesting an accumulation of lipid droplets (LD) which we confirmed via BODIPY 493/503 neutral lipid staining. Previous studies have shown that LDs are tightly linked to cell cycle progression, particularly in the G1/S phase transition, either by increasing their interaction with the mitochondria and peroxisomes, or to microtubules, to energetically fuel cell proliferation and promote cell survival through increased fatty acid oxidation, or to maintain lipid homoeostasis for efficient cell division [49]. More recently, perFAO has been shown to prevent lipotoxicity by regulating lipolysis from LDs via control of ATGL protein levels [50]. Alterations in membrane lipid composition have also been implicated to alter membrane properties such as membrane fluidity, in a way that promotes survival and treatment resistance in cancer cells [51]. This can be attributed to changes in the desaturation ratio of membrane lipids, increased SM and/or cholesterol content, and the formation of detergent-resistant membrane domains that can activate multi-drug efflux transporters [52]. Acyl-chain lengths can also have a profound impact on curvature, fluidity, and fusion rates of biological membranes, although the biological roles of different chain lengths and their regulation are less understood. Some possibilities include remodelling and expanding the endoplasmic reticulum (ER) [53], and mobilisation of lipids from LD stores [43, 54], supporting the idea that membrane synthesis and integrity could have potential impacts on cell division. In PCa, it was recently shown that fatty acid chain elongation via ELOVL5 promotes prostate tumour growth [55]. Future work is warranted to explore in detail and dissect the specific roles of DECR2 in these activities and the possibilities that these functional pathways intersect in order to drive tumour progression.

Besides uncovering a fundamental role for DECR2 in regulating lipid homoeostasis and cell cycle regulation, this study highlights the importance of perFAO for the first time in the emergence of CRPC or treatment resistance. Our findings are the first to suggest that abnormal perFAO is likely to be one of the contributing factors for resistance of PCa to enzalutamide. Herein, we showed that combination of DECR2 inhibition or TDZ with enzalutamide further abrogated PCa cell proliferation of 22Rv1, V16D and MR49F PCa cells and overexpression of DECR2 confers LNCaP cells to be more resistant to enzalutamide. Interestingly, a study by Shen et al. reported that BRAF mutant melanoma 'persister' cells resistant to BRAF/MEK inhibition switch their metabolism from glycolysis to oxidative phosphorylation that is predominantly dependent on perFAO compared to mitochondrial β-oxidation [21]. Peroxisomal-derived ether-linked phospholipids have been shown to drive susceptibility to and evasion from ferroptosis [56]. Gajewski et al. found that DECR2 loss promotes the resistance of tumour cells to immunotherapy by evading CD8 + T-cell-mediated tumour ferroptosis in vivo [57]. This suggests that low DECR2 expression may be advantageous to promote tumour growth, which is contradictory to our current findings. More extensive work will be needed to understand the diversity of mechanisms involved in the regulation of DECR2 in PCa progression and treatment resistance. It is important to recognise that peroxisomes do not function as an isolated entity. Organelle crosstalk and functional interplay exists between peroxisomes and many organelles such as the mitochondria, ER, lipid droplets and lysosomes to maintain metabolic homoeostasis [58]. A major challenge will be to reveal the mechanisms that mediate the metabolic interplay between peroxisomes and other organelles, and how these are impacted in various diseases/disorders. Our study also extends the current focus of peroxisome-mediated lipid changes in cancer cells to exploring the contribution of peroxisomes to tumorigenesis in the tumour microenvironment (i.e. immunity and inflammation [44, 59, 60], potentially opening up new therapeutic avenues to fight tumour cell proliferation by targeting peroxisome-related processes. Collectively, our findings make a new contribution to the study of altered lipid metabolism in PCa and reveals DECR2 as a major modulator of cell cycle progression and lipid metabolism, and an exciting novel candidate for therapeutic targeting.

DATA AVAILABILITY

Raw RNA sequencing data are available through NCBI's Gene Expression Omnibus under the accession number GSE218282. Other data sets generated and/or analysed during this study are included in the Supplementary Table files.

REFERENCES

1. Siegel RL, Miller KD, Jemal A. Cancer statistics, 2019. CA Cancer J Clin. 2019;69:7–34.
2. Ahmad F, Cherukuri MK, Choyke PL. Metabolic reprogramming in prostate cancer. Br J Cancer. 2021;125:1185–96.
3. Watt MJ, Clark AK, Selth LA, Haynes VR, Lister N, Rebello R, et al. Suppressing fatty acid uptake has therapeutic effects in preclinical models of prostate cancer. Sci Transl Med. 2019;11:eaau5758.
4. Zadra G, Ribeiro CF, Chetta P, Ho Y, Cacciatore S, Gao X, et al. Inhibition of de novo lipogenesis targets androgen receptor signaling in castration-resistant prostate cancer. Proc Natl Acad Sci USA. 2019;116:631–40.
5. Nassar ZD, Mah CY, Centenera MM, Irani S, Sadowski MC, Scott JS, et al. Fatty acid oxidation is an adaptive survival pathway induced in prostate tumors by HSP90 inhibition. Mol Cancer Res. 2020;18:1500–11.
6. Balaban S, Nassar ZD, Zhang AY, Hosseini-Beheshti E, Centenera MM, Schreuder M, et al. Extracellular fatty acids are the major contributor to lipid synthesis in prostate cancer. Mol Cancer Res. 2019;17:949–62.
7. Schlaepfer IR, Rider L, Rodrigues LU, Gijón MA, Pac CT, Romero L, et al. Lipid catabolism via CPT1 as a therapeutic target for prostate cancer. Mol Cancer Ther. 2014;13:2361–71.
8. Nassar ZD, Mah CY, Dehairs J, Burvenich IJ, Irani S, Centenera MM, et al. Human DECR1 is an androgen-repressed survival factor that regulates PUFA oxidation to protect prostate tumor cells from ferroptosis. Elife. 2020;9:e54166.
9. Ananthanarayanan V, Deaton RJ, Yang XJ, Pins MR, Gann PH. Alpha-methylacyl-CoA racemase (AMACR) expression in normal prostatic glands and high-grade prostatic intraepithelial neoplasia (HGPIN): association with diagnosis of prostate cancer. Prostate. 2005;63:341–6.
10. Jiang Z, Woda BA, Wu C-L, Yang XJ. Discovery and clinical application of a novel prostate cancer marker: alpha-methylacyl CoA racemase (P504S). Am J Clin Pathol. 2004;122:275–89.
11. Itkonen HM, Brown M, Urbanucci A, Tredwell G, Ho Lau C, Barfeld S, et al. Lipid degradation promotes prostate cancer cell survival. Oncotarget. 2017;8:38264–75.
12. Toren P, Kim S, Johnson F, Zoubeidi A. Combined AKT and MEK pathway blockade in pre-clinical models of enzalutamide-resistant prostate cancer. PLoS One. 2016;11:e0152861.
13. Cerami E, Gao J, Dogrusoz U, Gross BE, Sumer SO, Aksoy BA, et al. The cBio cancer genomics portal: an open platform for exploring multidimensional cancer genomics data. Cancer Discov. 2012;2:401–4.
14. Taylor BS, Schultz N, Hieronymus H, Gopalan A, Xiao Y, Carver BS, et al. Integrative genomic profiling of human prostate cancer. Cancer Cell. 2010;18:11–22.
15. Grasso CS, Wu Y-M, Robinson DR, Cao X, Dhanasekaran SM, Khan AP, et al. The mutational landscape of lethal castration-resistant prostate cancer. Nature. 2012;487:239–43.
16. Tomlins SA, Mehra R, Rhodes DR, Cao X, Wang L, Dhanasekaran SM, et al. Integrative molecular concept modeling of prostate cancer progression. Nat Genet. 2007;39:41–51.
17. Blomme A, Ford CA, Mui E, Patel R, Ntala C, Jamieson LE, et al. 2,4-dienoyl-CoA reductase regulates lipid homeostasis in treatment-resistant prostate cancer. Nat Commun. 2020;11:2508.
18. Piccinini F, Tesei A, Arienti C, Bevilacqua A. Cancer multicellular spheroids: volume assessment from a single 2D projection. Comput Methods Prog Biomed. 2015;118:95–106.
19. Merico D, Isserlin R, Stueker O, Emili A, Bader GD. Enrichment map: a network-based method for gene-set enrichment visualization and interpretation. PLoS One. 2010;5:e13984.
20. Van den Branden C, Roels F. Thioridazine: a selective inhibitor of peroxisomal beta-oxidation in vivo. FEBS Lett. 1985;187:331–3.
21. Shen S, Faouzi S, Souquere S, Roy S, Routier E, Libenciuc C, et al. Melanoma persister cells are tolerant to BRAF/MEK inhibitors via ACOX1-mediated fatty acid oxidation. Cell Rep. 2020;33:108421.
22. Purhonen M, Koponen H, Tiihonen J, Tanskanen A. Outcome of patients after market withdrawal of thioridazine: a retrospective analysis in a nationwide cohort. Pharmacoepidemiol Drug Saf. 2012;21:1227–31.
23. Shi R, Zhang Y, Shi Y, Shi S, Jiang L. Inhibition of peroxisomal β-oxidation by thioridazine increases the amount of VLCFAs and Aβ generation in the rat brain. Neurosci Lett. 2012;528:6–10.
24. Centenera MM, Hickey TE, Jindal S, Ryan NK, Ravindranathan P, Mohammed H, et al. A patient-derived explant (PDE) model of hormone-dependent cancer. Mol Oncol. 2018;12:1608–22.
25. Beltran H, Prandi D, Mosquera JM, Benelli M, Puca L, Cyrta J, et al. Divergent clonal evolution of castration-resistant neuroendocrine prostate cancer. Nat Med. 2016;22:298–305.
26. Keenan AB, Torre D, Lachmann A, Leong AK, Wojciechowicz ML, Utti V, et al. ChEA3: transcription factor enrichment analysis by orthogonal omics integration. Nucleic Acids Res. 2019;47:W212–24.
27. Islinger M, Voelkl A, Fahimi HD, Schrader M. The peroxisome: an update on mysteries 2.0. Histochem Cell Biol. 2018;150:443–71.
28. Molenaar MR, Jeucken A, Wassenaar TA, van de Lest CHA, Brouwers JF, Helms JB. LION/web: a web-based ontology enrichment tool for lipidomic data analysis. Gigascience. 2019;8:giz061.
29. Abida W, Cyrta J, Heller G, Prandi D, Armenia J, Coleman I, et al. Genomic correlates of clinical outcome in advanced prostate cancer. Proc Natl Acad Sci USA. 2019;116:11428–36.
30. Duval K, Grover H, Han L-H, Mou Y, Pegoraro AF, Fredberg J, et al. Modeling physiological events in 2D vs. 3D cell culture. Physiol (Bethesda). 2017;32:266–77.
31. Tegowski M, Fan C, Baldwin AS. Selective effects of thioridazine on self-renewal of basal-like breast cancer cells. Sci Rep. 2019;9:18695.
32. Kim J-A. Peroxisome metabolism in cancer. Cells. 2020;9:1692.
33. Zalckvar E, Schuldiner M. Beyond rare disorders: a new era for peroxisomal pathophysiology. Mol Cell. 2022;82:2228–35.
34. Alphey MS, Yu W, Byres E, Li D, Hunter WN. Structure and reactivity of human mitochondrial 2,4-dienoyl-CoA reductase: enzyme-ligand interactions in a distinctive short-chain reductase active site. J Biol Chem. 2005;280:3068–77.
35. De Nys K, Meyhi E, Mannaerts GP, Fransen M, Van Veldhoven PP. Characterisation of human peroxisomal 2,4-dienoyl-CoA reductase. Biochim Biophys Acta. 2001;1533:66–72.
36. Hua T, Wu D, Ding W, Wang J, Shaw N, Liu Z-J. Studies of human 2,4-dienoyl CoA reductase shed new light on peroxisomal β-oxidation of unsaturated fatty acids. J Biol Chem. 2012;287:28956–65.
37. Spiegel A, Lauber C, Bachmann M, Heninger A-K, Klose C, Simons K, et al. A set of gene knockouts as a resource for global lipidomic changes. Sci Rep. 2022;12:10533.
38. Köberlin MS, Snijder B, Heinz LX, Baumann CL, Fauster A, Vladimer GI, et al. A conserved circular network of coregulated lipids modulates innate immune responses. Cell. 2015;162:170–83.
39. Atilla-Gokcumen GE, Muro E, Relat-Goberna J, Sasse S, Bedigian A, Coughlin ML, et al. Dividing cells regulate their lipid composition and localization. Cell. 2014;156:428–39.
40. Guo T, Gregg C, Boukh-Viner T, Kyryakov P, Goldberg A, Bourque S, et al. A signal from inside the peroxisome initiates its division by promoting the remodeling of the peroxisomal membrane. J Cell Biol. 2007;177:289–303.
41. Herzog K, Pras-Raves ML, Vervaart MAT, Luyf ACM, van Kampen AHC, Wanders RJA, et al. Lipidomic analysis of fibroblasts from Zellweger spectrum disorder patients identifies disease-specific phospholipid ratios. J Lipid Res. 2016;57:1447–54.
42. Lodhi IJ, Semenkovich CF. Peroxisomes: a nexus for lipid metabolism and cellular signaling. Cell Metab. 2014;19:380–92.
43. Sanchez-Alvarez M, Zhang Q, Finger F, Wakelam MJO, Bakal C. Cell cycle progression is an essential regulatory component of phospholipid metabolism and membrane homeostasis. Open Biol. 2015;5:150093.
44. Nath AS, Parsons BD, Makdissi S, Chilvers RL, Mu Y, Weaver CM, et al. Modulation of the cell membrane lipid milieu by peroxisomal β-oxidation induces Rho1 signaling to trigger inflammatory responses. Cell Rep. 2022;38:110433.
45. Francis M, Abou Daher A, Azzam P, Mroueh M, Zeidan YH. Modulation of DNA damage response by sphingolipid signaling: an interplay that shapes cell fate. Int J Mol Sci. 2020;21:4481.
46. Sanidas I, Morris R, Fella KA, Rumde PH, Boukhali M, Tai EC, et al. A code of mono-phosphorylation modulates the function of RB. Mol Cell. 2019;73:985–1000.e6
47. Muranaka H, Hayashi A, Minami K, Kitajima S, Kohno S, Nishimoto Y, et al. A distinct function of the retinoblastoma protein in the control of lipid composition identified by lipidomic profiling. Oncogenesis. 2017;6:e350.
48. Takahashi C, Sasaki N, Kitajima S. Twists in views on RB functions in cellular signaling, metabolism and stem cells. Cancer Sci. 2012;103:1182–8.
49. Cruz ALS, Carrossini N, Teixeira LK, Ribeiro-Pinto LF, Bozza PT, Viola JPB. Cell cycle progression regulates biogenesis and cellular localization of lipid droplets. Mol Cell Biol. 2019;39:e00374-18.
50. Ding L, Sun W, Balaz M, He A, Klug M, Wieland S, et al. Peroxisomal β-oxidation acts as a sensor for intracellular fatty acids and regulates lipolysis. Nat Metab. 2021;3:1648–61.
51. Rysman E, Brusselmans K, Scheys K, Timmermans L, Derua R, Munck S, et al. De novo lipogenesis protects cancer cells from free radicals and chemotherapeutics by promoting membrane lipid saturation. Cancer Res. 2010;70:8117–26.
52. Kopecka J, Trouillas P, Gašparović AČ, Gazzano E, Assaraf YG, Riganti C. Phospholipids and cholesterol: Inducers of cancer multidrug resistance and therapeutic targets. Drug Resist Updat. 2020;49:100670.
53. Volmer R, van der Ploeg K, Ron D. Membrane lipid saturation activates endoplasmic reticulum unfolded protein response transducers through their transmembrane domains. Proc Natl Acad Sci USA. 2013;110:4628–33.
54. Krahmer N, Guo Y, Wilfling F, Hilger M, Lingrell S, Heger K, et al. Phosphatidylcholine synthesis for lipid droplet expansion is mediated by localized activation of CTP:phosphocholine cytidylyltransferase. Cell Metab. 2011;14:504–15.

55. Centenera MM, Scott JS, Machiels J, Nassar ZD, Miller DC, Zinonos I, et al. ELOVL5 is a critical and targetable fatty acid elongase in prostate cancer. Cancer Res. 2021;81:1704–18.
56. Zou Y, Henry WS, Ricq EL, Graham ET, Phadnis VV, Maretich P, et al. Plasticity of ether lipids promotes ferroptosis susceptibility and evasion. Nature. 2020;585:603–8.
57. Gajewski T, Higgs E, Li S, Flood B, Hatogai K. 239 Decr2 loss promotes resistance of tumor cells to immunotherapy by affecting CD8+ T cell-regulated tumor ferroptosis. J Immunother Cancer. 2020;8:A257–A257.
58. Schrader M, Kamoshita M, Islinger M. Organelle interplay-peroxisome interactions in health and disease. J Inherit Metab Dis. 2020;43:71–89.
59. Di Cara F, Andreoletti P, Trompier D, Vejux A, Bülow MH, Sellin J, et al. Peroxisomes in immune response and inflammation. Int J Mol Sci. 2019;20:3877.
60. Di Cara F, Sheshachalam A, Braverman NE, Rachubinski RA, Simmonds AJ. Peroxisome-mediated metabolism is required for immune response to microbial infection. Immunity. 2017;47:93–106.e7

ACKNOWLEDGEMENTS

The results published here are in part based on data generated by The Cancer Genome Atlas, established by the National Cancer Institute and the National Human Genome Research Institute, and we are grateful to the specimen donors and relevant research groups associated with this project. Tissues for the patient-derived explants used in the study were collected at St Andrew's Hospital, Adelaide, with informed consent via the Australian Prostate Cancer BioResource and we thank the doctors, patients and health care professionals involved. We acknowledge expert technical assistance in the study from Samira Khabbazi. Flow cytometry analysis was performed at the South Australian Health Medical Research Institute (SAHMRI) in the ACRF Cellular Imaging and Cytometry Core Facility, generously supported by the Australian Cancer Research Foundation, Detmold Hoopman Group and Australian Government through the Zero Childhood Cancer Programme. The authors acknowledge the South Australian Genomics Centre (SAGC) which provided the RNA-sequencing services. The SAGC is supported by the National Collaborative Research Infrastructure Strategy (NCRIS) via BioPlatforms Australia and by the SAGC partner institutes. Animal studies were performed at the Bioresources Facilities at the South Australian Health and Medical Research Institute. The authors also thank Adelaide Microscopy (University of Adelaide). Metabolomics was facilitated by access to Sydney Mass Spectrometry, core research facility at the University of Sydney. Mah, C.Y., Nguyen, A.D.T., Niijima, T., Helm, M., Dehairs, J., Ryan, F.J. et al. Peroxisomal β-oxidation enzyme, DECR2, regulates lipid metabolism and promotes treatment resistance in advanced prostate cancer. bioRxiv, Preprint posted online 5 November 2022, https://doi.org/10.1101/2022.11.05.515262 (2022). The research programmes of LMB, AJH, and JVS are supported by the Movember Foundation and the Prostate Cancer Foundation of Australia through a Movember Revolutionary Team Award (MRTA3). CYM is supported by an Early-Career Future Leaders Research Fellowship awarded by the Prostate Cancer Foundation of Australia. AJH is supported by a Robinson Fellowship and funding from the University of Sydney. DJL is supported by an EMBL Australia Group Leader Award. JVS is supported by a KU Leuven CI Grant (C14/21/095) and the Belgian Foundation Against Cancer (STK; F/2020/1417). LMB is supported by a Principal Cancer Research Fellowship awarded by Cancer Council's Beat Cancer project on behalf of its donors, the State Government through the Department of Health and the Australian Government through the Medical Research Future Fund (PRF1117). ZDN is supported by Cancer Australia (ID2011672) and the U.S. Department of Defense (PC210356). ZDN and LMB are supported by the Hospital Research Foundation (C-PJ-10-Prost-2020).

AUTHOR CONTRIBUTIONS

CYM, ZDN and LMB conceived the study and wrote the manuscript. CYM, MH, AJH, LQ, DJL, JD and JVS designed experiments. CYM, ADTN, TN, JD, NR, AJH, LQ, ASD and JVS acquired data and performed experiments. CYM, ADTN, TN, IGM, FR, DJL, AJH, LQ and ASD interpreted and analysed the data. DJL, ZDN and LMB supervised the study. JVS, ZDN and LMB acquired funding. MH and CYM performed the in vivo experiments. All authors read the manuscript, agreed with the content, and were given the opportunity to provide input.

FUNDING

Open Access funding enabled and organized by CAUL and its Member Institutions.

COMPETING INTERESTS

The authors declare no competing interests.

ETHICS APPROVAL

Prostate cancer tissues were collected from men undergoing robotic radical prostatectomy at St. Andrew's Hospital (Adelaide, Australia) with written informed consent through the Australia Prostate Cancer BioResource. Ethical approval for the use of human prostate tumours was obtained from the Ethics Committees of the University of Adelaide (Adelaide, Australia; approval H-2012-016) and St Andrew's Hospital (Adelaide, Australia; approval 80). The orthotopic xenograft studies were approved by the South Australian Health and Medical Research Institute Animal Ethics Committee (approval number SAM442.19). All procedures were carried out in accordance with the guidelines of the National Health and Medical Research Council of Australia.

ADDITIONAL INFORMATION

Supplementary information The online version contains supplementary material available at https://doi.org/10.1038/s41416-023-02557-8.

Correspondence and requests for materials should be addressed to Zeyad D. Nassar or Lisa M. Butler.

Reprints and permission information is available at http://www.nature.com/reprints

Publisher's note Springer Nature remains neutral with regard to jurisdictional claims in published maps and institutional affiliations.